COMPRESSIVE STOCKING OPTIMIZATION FOR LOWER LIMB LYMPHEDEMA TREATMENT

A. GARCIA-LLONA[1], M. AGUIRRE[2], F. VERDUGO[3] AND S. AVRIL[1]

[1] Mines Saint-Etienne
U 1059 Sainbiose, F-42023 Saint-Etienne, France
aratz.garciallona, avril@emse.fr

[2] Laboratori de Càlcul Numèric, Universitat Politècnica de Catalunya
Jordi Girona 1, E-08034, Barcelona, Spain
miquel.aguirre@upc.edu

[3] Department of Computer Science, Universiteit Amsterdam
De Boelelaan 1111, 1081 HV Amsterdam, The Netherlands
f.verdugo.rojano@vu.nl

Key words: Lymphedema, Reduced Order Model, Adaptive sampling, Finite Element Method.

Abstract. Lymphedema is a chronic disease that causes swelling in the soft tissues, mostly taking place in the extremities. This research focuses on the treatment of lymphedema through compression, which is widely applied to reduce the volume of edemas. Although effective at a clinical level, the use of off-the-shelf stockings with predefined sizes, reduces the efficiency at the patient-specific level. With the long-term goal of designing patient-specific stockings, this study aims to develop a real-time simulation tool, able to predict the efficiency of a given compression stocking for a given patient. For such purpose, the use of standard Finite Element Method (FEM) falls short due to high computational cost. Therefore, a solution based on Reduced Order Modeling (ROM) is developed to compute, in real-time, the hydrostatic pressure distribution at the location of the lymphatic dysfunction. It is assumed that hydrostatic pressure improves lymph circulation and increase the drainage capacity. This method enables to design the most efficient compressive stockings considering the particularities of each patient.

1 INTRODUCTION

The lymphatic system is formed by lymph nodes and lymphatic vessels that collect and carry lymph fluid through the body. Lymphedema is a chronic disorder of the lymphatic system and is a debilitating condition that greatly impacts patients' daily well-being. The lymphatic vessels are not able to drain the lymph which tends to cause fluid retention (edema). This induces the swelling of soft tissues, which usually takes place at the extremities, legs and arms [1]. There are two types of lymphedema: i) the primary lymphedema, which occurs due to genetic disorders [2] ii) the secondary lymphedema, which results from external factors, such as cancer treatment

where the lymphatic system is damaged or lymph nodes are removed. This article focuses on secondary lymphedema in the lower limbs, affecting one over 1,000 individuals [3, 4, 5].

Compression stockings are widely used to promote healthy lymph flow and decrease swelling in the lower-limb [6, 7, 8, 9]. The application of adequate compression reduces the cross-section of the vessels, which improves the lymphatic drainage. These stockings typically come in standardized sizes, which reduces their effectiveness. A patient-specific solution could increase the effectiveness by taking into account patient-specific features such as the severity of the lymphedema and the morphology of the patient [10, 11, 12].

We propose a patient-specific approach based on digital twins to study these effects. Digital twins have been largely developed in different medical fields for diagnosis, treatment decision and long-term prediction at health outcomes [13, 14, 15]. A digital twin of the lower-limb can provide valuable information in real-time to design the most effective compression stockings. It enables to analyze the stress distribution in the soft tissues, which plays a key role in the lymph drainage. Such complex mechanical problem requires solving nonlinear solid mechanics equilibrium equations considering many geometrical variables, material parameters and boundary conditions. It is not affordable to solve a model for each patient applying traditional numerical tools such as Finite Element Method (FEM) due to the high computational-cost.

The aim of ROM techniques is to replace the original large-dimension numerical problem by a problem of smaller dimension, which provides a reliable and fast approximation of the solution [16, 17, 18, 19]. In this study non-intrusive ROM is applied to compute the stresses in the soft tissues. The ROM is derived through the resolution of several FE models or high-fidelity models defined by a set of patient-specific parameters. The approach to reduce the full-order model consists in the projection of the high-fidelity solutions upon a low dimensional space defined with specially selected basis functions. This is achieved through Proper Orthogonal Decomposition (POD), which decomposes the high fidelity solution in a linear combination of a set of coefficients and modes. In order to reconstruct the approximate solution, the POD coefficients should be predicted using surrogate models. This method is known as Proper Orthogonal Decomposition with Interpolation (PODI) [20, 21, 22]. For a new set of parameters the POD coefficients are interpolated and the approximated solution is computed (online-stage).

The aim of this work is to predict in real-time the hydrostatic pressures in the soft tissues surrounding the lymphatic vessels. This work focuses on the geometrical variables, whilst material properties and boundary conditions are kept constant. PODI is applied to estimate the hydrostatic pressure for a given set of geometrical parameters. The main drawback of non-intrusive ROMs is the high computational cost of the offline-stage. In this research an adaptive-sampling method is proposed to solve the full-order model as fast as possible by selecting the most efficient set of parameters, instead of the widely used static sampling methods such as Latin hypercube sampling.

The article is structured as follows. Section 2 presents the algorithm to carry out the digital twin of the lower-limb. In Section 3 a numerical example is presented and the adaptive sampling algorithm is analyzed. Lastly, the conclusions and future perspective are presented in Section 4.

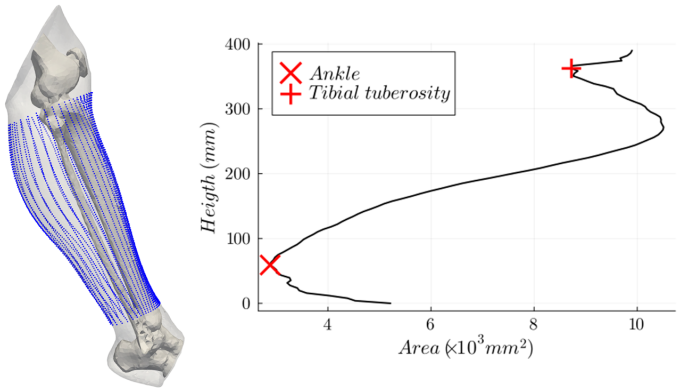

Figure 1: Lower-limb definition

2 METHOD

2.1 Finite Element Method

The studied part of the lower limb is limited between the ankle and the tibial tuberosity. This region is defined geometrically by the global and local minimum of the Area/Heigth curve as shown in Figure 1. Once the geometry is defined, the mesh of the studied part of the leg is generated to carry out the FE simulation.

The constitutive behavior of the soft tissues of the lower limb is modeled with a compressible Neo-Hookean material [23, 24, 25]. The strain energy density function is defined as:

$$\Psi(\boldsymbol{C}) = \frac{\lambda_0}{2}\left(lnJ\right)^2 - \mu_0\, lnJ + \frac{\mu_0}{2}\left[trace\left(\boldsymbol{C}\right) - 3\right] \tag{1}$$

which yields the following Cauchy stress tensor:

$$\boldsymbol{\sigma} = \lambda_0\, lnJ\, \boldsymbol{C}^{-1} + \mu_0\left(\boldsymbol{I} - \boldsymbol{C}^{-1}\right) \tag{2}$$

λ_0 and μ_0 are the Lamé parameters, $J = det\left(\boldsymbol{F}\right)$, $\boldsymbol{F}$ is the deformation gradient, $\boldsymbol{C}$ is the right Cauchy-Green tensor and $\boldsymbol{I}$ is the identity tensor.

As this research work focuses on the geometrical aspects, material properties and boundary conditions are kept constant. Two hyperelastic materials are considered, muscle ($E_M = 33.18\ kPa$ and $\nu_M = 0.49$) and fat ($E_F = 17.37\ kPa$ and $\nu_F = 0.49$) [24]. The bones (tibia and fibula) are assumed as perfectly rigid and their movement are constrained at the surface of the bones. We also constrain the vertical displacement of the top and bottom surface of the model because the compression pressure cannot cause the lengthening or shortening of the lower leg. Regarding the force boundary conditions, normal and uniform pressure of 3 kPa is applied over the surface of the leg, corresponding to a standard compression therapy [24, 28].

The FE analysis was carried out using Gridap which is a free and open source FE library written in Julia [26].

2.2 Reduced Order Model: PODI

In this research work, PODI is applied to identify the most relevant features. The proposed approach consists in two stages: offline and online stage. In the offline stage, full-order models are solved (FE Method) for different sets of parameters, $\boldsymbol{\mu} = [\boldsymbol{\mu}_1, \boldsymbol{\mu}_2, ..., \boldsymbol{\mu}_{Ns}]$ where $\boldsymbol{\mu}_i = [\mu_i^1, \mu_i^2, ..., \mu_i^{N_p}]$. The computed results are saved in the snapshots matrix $\boldsymbol{S}(\boldsymbol{\mu}) = [\boldsymbol{s}_1, \boldsymbol{s}_2, ..., \boldsymbol{s}_{Ns}]$. The POD is computed applying singular value decomposition of the snapshots matrix:

$$svd(\boldsymbol{S}) = \boldsymbol{\Psi}, \boldsymbol{\Sigma}, \boldsymbol{V^T} \tag{3}$$

The number of basis (L) is defined using the singular values $\boldsymbol{\Sigma} = [\sigma_1, \sigma_2, ..., \sigma_{Ns}]$ to retain the dominant or the most energetic modes ($\boldsymbol{\Psi}$):

$$\frac{\sum_{i=1}^{L} \sigma_i^2}{\sum_{i=1}^{N_s} \sigma_i^2} < \delta_{tol} \rightarrow L \tag{4}$$

The approximate solution is computed using the POD modes or basis vector ($\boldsymbol{\Psi}$) and POD coefficients $\alpha_j = S\Psi_j$ of the most dominant modes:

$$\boldsymbol{s}_i \approx \tilde{\boldsymbol{s}}_i = \sum_{j=1}^{L} \alpha_j \Psi_j \tag{5}$$

The POD coefficients and the parameters are used to build the surrogate model by applying an interpolation method. Radial basis function interpolation method enables to estimate α^* for any parameter during the online stage. Therefore, the solution can be computed using the interpolated α^* while running the FE model is avoided.

$$\boldsymbol{s}^* = \sum_{j=1}^{L} \alpha_j^* \Psi_j \tag{6}$$

2.3 Adaptive sampling

The adaptive sampling methods are based on exploration-exploitation dilemma to select new sampling points. Exploitation consists in placing sampling points in subregions, which have been identified as demanding for accuracy based on the computed FE solution. It is a very conservative method because it selects new samples near the outstanding sample points that already exist. The main drawback of a full-exploitation method is that it prevents discovering potential regions where new sample points can be selected. In this research work, a cross-validation method is used to estimate the sensitivity of each sampling point and more specifically the Leave-One-Out Cross-validation (LOOCV). There is no clear criterion to select the initial size N_μ of the sampling-set $\boldsymbol{\mu}$ [27]. The snapshot matrix $\boldsymbol{S}$ is defined by solving the FE model for

each sample. Then, the reduced order model s^* is computed removing the sample μ_i from the sampling-set as it is explained in Algorithm 1. The LOOCV error is defined as:

$$e_{LOOCV}(\boldsymbol{\mu}_i) = \|\boldsymbol{S}(\boldsymbol{\mu}_i) - \boldsymbol{s}^*_{-i}(\boldsymbol{\mu}_i)\| \tag{7}$$

which measures the sensitivity of losing one sampling point. High values of e_{LOOCV} indicates that there is a lack of information or observations near the removed sampling point and introducing sampling points in this region could improve the accurateness of the reduced order model s^*. Then, the interpolation model of LOOCV error e^*_{LOOCV} is defined using the radial basis function (RBF) and the computed e_{LOOCV} at the sampling points.

On the other hand, exploration aims to propose new sample points considering the fact that the observed data is not sufficient. This strategy allows to identify new regions preventing local clustering. However, it could happen that does not provide sample points at the identified critical regions or it leads to sample points with poor information. In this work, a discontinuous distance-based exploration approach is applied. The parameter space is divided into the number of existing samples applying the Voronoi tessellation. The new sample μ_{new} belongs to the cell relative to the closest existing samples μ. The distance metric is measured as:

$$d_{min}(\boldsymbol{\mu}_{new}) = min_{\boldsymbol{\mu}_{new}}(\|\boldsymbol{\mu}_{new} - \boldsymbol{\mu}\|) \tag{8}$$

High values of d_{min} means that the sample point is far away from the N_μ samples that already defines the sampling set $\boldsymbol{\mu}$.

The goal of adaptive sampling is to find a sampling point with a good trade-off between these two strategies. The new sampling point should be placed as far as possible from the existing samples to achieve space filling condition (exploration) and its impact would be the highest (exploitation). The new sampling point is computed minimizing the following loss function,

$$L(\boldsymbol{\mu}) = -e^*_{LOOCV}(\boldsymbol{\mu})\ d_{min}(\boldsymbol{\mu})\ \delta(\boldsymbol{\mu}) \tag{9}$$

where $L(\boldsymbol{\mu})$ is the egg-holder shape function which is difficult to optimize because there are many local minima. Different initial points are tried to ensure that the global minimum is found. The new sample $\boldsymbol{\mu}_{new}$ is defined by minimizing the loss function through the Adam optimizer. Algorithm 1 summarizes the proposed adaptive sampling.

3 RESULTS

The adaptive sampling performance is evaluated using a simplified geometry which facilitate the performance analysis of the proposed methodology. The template leg is deformed based on two variables $\boldsymbol{\mu_i} = (\mu_i^1, \mu_i^2)$ where $\mu_i^1 \in [-0.20,\ 0.30]$ and $\mu_i^2 \in [-0.05,\ 0.20]$. The template leg is deformed transversely while the length of the leg is kept constant. To this end the control points are grouped in two: internal (green color) and external (yellow color) control points, as showed in Figure 2. The two sets of points are moved in the XY plane based in the selected parameters $\boldsymbol{\mu_i}$ to get the target mesh. Figure 2 shows the target mesh computed for

Algorithm 1 Adaptive sampling algorithm

0: **INPUT:** $\boldsymbol{S}$, $\boldsymbol{\mu}$
0: **for** $\boldsymbol{\mu}_i$ in $\boldsymbol{\mu}$ **do** {Exploitation stage}
0: remove $\boldsymbol{s}_i(\boldsymbol{\mu}_i)$ from $\boldsymbol{S}$
0: compute ROM $\rightarrow \boldsymbol{s}^*_{-i}(\boldsymbol{\mu}_i)$
0: compute error $e_{LOOCV}(\boldsymbol{\mu}_i)$
0: **end for**
0: interpolation model $e^*_{LOOCV}(\tilde{\boldsymbol{\mu}})$
0: distance-based exploration $d_{min}(\tilde{\boldsymbol{\mu}})$ {Exploration stage}
0: define loss function $L(\tilde{\boldsymbol{\mu}}) = -e^*_{LOOCV}(\tilde{\boldsymbol{\mu}})\ d_{min}(\tilde{\boldsymbol{\mu}})\ \delta(\tilde{\boldsymbol{\mu}})$
0: minimize $L(\tilde{\boldsymbol{\mu}}) \rightarrow \boldsymbol{\mu}_{new}$
0: update $\boldsymbol{\mu}$ with $\boldsymbol{\mu}_{new}$
0: **OUTPUT:** $\boldsymbol{\mu}$ =0

$\mu = [0.15, -0.02]$, where 0.15 and -0.02 parameterized the displacement of the external and internal control points respectively.

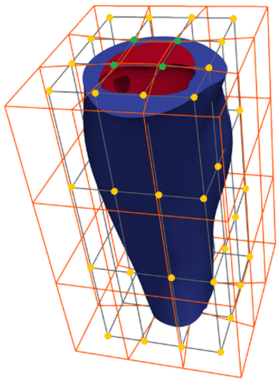

Figure 2: Lower-limb definition

With the objective of solving the FE model with the lowest cost possible, the sampling algorithm presented in Algorithm 1 is applied to select μ_{new}. The initial sample size is selected as $N^0_\mu = 9$ and N_c new sampling points are selected applying Algorithm 1. Figure 3 shows graphically the definition of the initial exploitation (e^*_{LOOCV}), exploration (d_{min}) and loss ($L(\mu)$) function defined by the initial sampling set. After minimizing the loss function, a new sampling point is computed.

Every time a sampling point is introduced, the function $d_{min}(\boldsymbol{\mu})$ is updated. However, the sensitivity function e^*_{LOOCV} is not updated until N_c sampling points are selected. The surface function $L(\boldsymbol{\mu})$ is modified every time a new sampling point is added. The new sampling point is selected by minimizing $L(\boldsymbol{\mu})$. Figure 4 shows the evolution of the loss function while new sampling points are introduced. After selecting N_c new sampling points, the FE model is solved

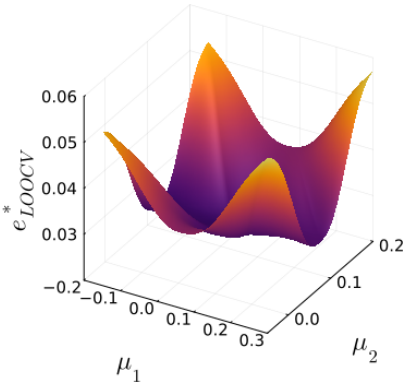

(a) Exploitation

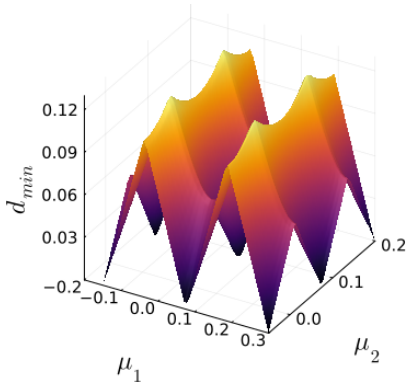

(b) Exploration

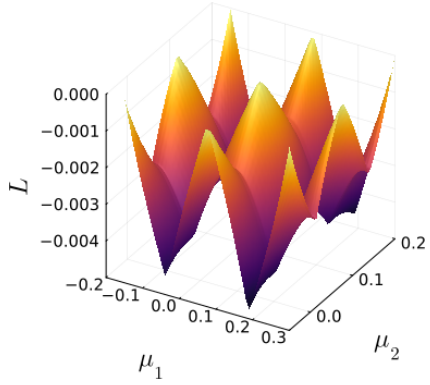

(c) Loss

Figure 3: Initial exploitation, exploration and loss surfaces ($N_\mu^0 = 9$)

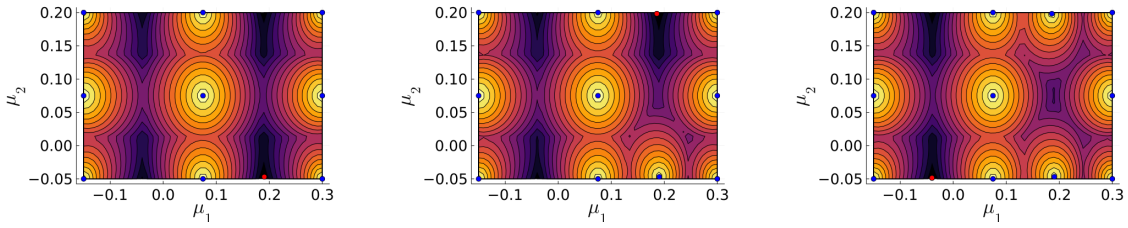

(a) 1^{st} sampling point (b) 2^{nd} sampling point (c) 3^{rd} sampling point

Figure 4: Adaptive sampling for $N_c = 3$

for each parameter combination, while the results of the FE model are used to build the new ROM.

The number of new sample points N_c is defined by the number of cores available on the cluster to take advantage of the computational resources available. This procedure is repeated until reaching the established tolerance. In this benchmark, it was used $N_c = 75$ cores and a tolerance of 0.1 % between the solution of the full-order model and the ROM. Following this criterion, 1,259 samples are required.

Once the sampling and the FEA are achieved, the ROM is defined with the PODI method. Figure 5 shows the linear combination of modes (Ψ_j) to compute the approximated solution (s^*). Considering $\delta_{tol} = 0.01\%$, L=5 modes is enough to compute the approximate solution. The ROM computes the displacement in every node which enables to derive the hydrostatic pressures through Equation 2.

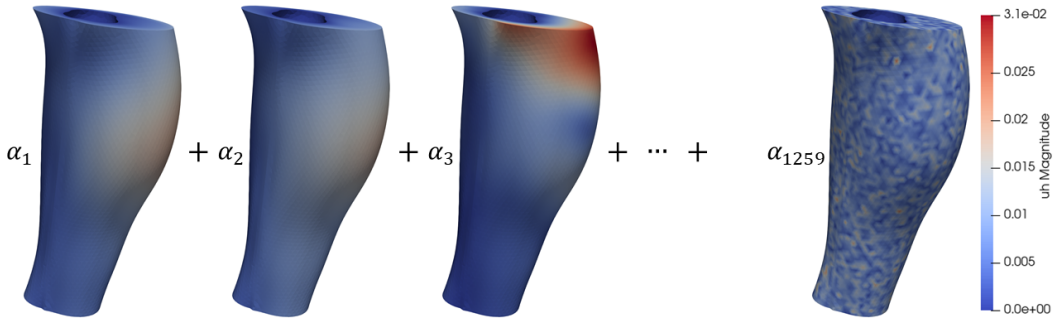

Figure 5: Proper orthogonal decomposition

The performance of the ROM is validated by comparing the solutions provided by the FEA and the ROM at 200 sampling points different from the ones used to create the ROM. Figure 6 shows the difference between the computed and the estimated hydrostatic pressures. The maximum error is 1.8 % while the mean error is about 0.1 %, which are sufficiently small. The developed ROM can be considered as an accurate tool to predict the hydrostatic pressures in the soft tissues of the lower limb.

The proposed numerical tool provides internal stress distributions (see Figure 7) resulting

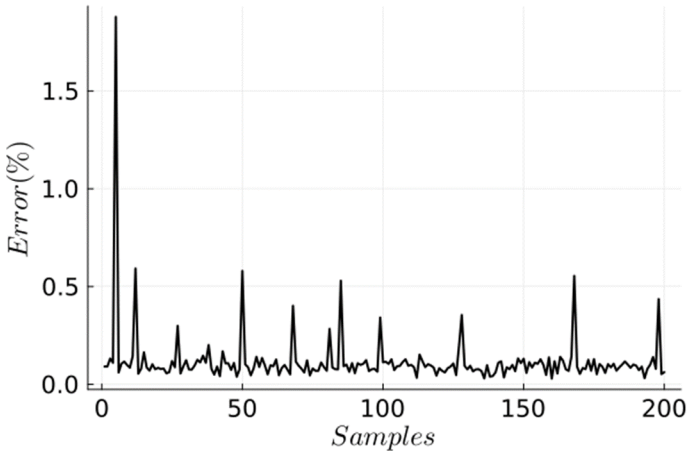

Figure 6: Comparison between full-order model solution and ROM solution

from the compressive therapy, which would be very difficult to estimate otherwise. In contrast with experimental tests such as elastography [29], the numerical tool enables to study the effect of different external pressures in a simple way. This advantage reduces the trial and error to look for the most efficient compressive stocking. This stress distribution is meaningful with respect to the improvement of lymph circulation. It also helps to design patient-specific stockings avoiding stress concentrations that can cause discomforts. These suppose a step forward to increase the efficiency of compressing stockings compared to the off-the-shelf stockings.

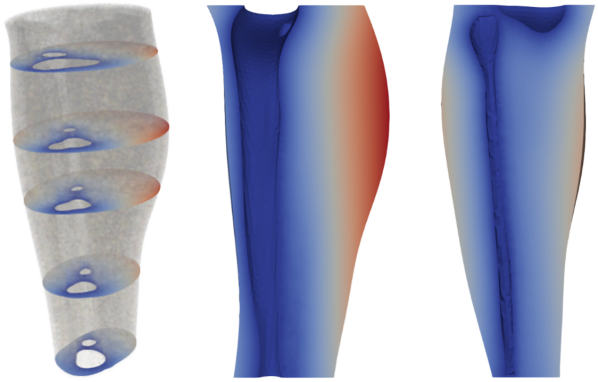

Figure 7: ROM solution

4 CONCLUSION

A digital twin of a lower-limb constitutes an essential numerical tool to carry out a patient-specific design of compression stockings for lymphedema treatment. An approach based on non-intrusive ROM has been proposed to achieve this objective. To reduce the computational cost of the offline stage of ROM, an adaptive sampling is proposed together with PODI. This

algorithm selects the full-order model where information is required to increase the accurateness of the ROM. This promising approach constitutes a step forward to support doctors and stocking manufacturers in their search of patient-specific solutions.

Future research into digital twin of the lower limb will consider material properties and boundary conditions. Furthermore, while other reduced order method such as kernel POD could be considered, low-cost and non-invasive methods should be studied to parametrize the lower-limb.

ACKNOWLEDGMENT

The authors wish to express their gratitude to BPI France for having funded this research work through the Symphonies Project.

REFERENCES

[1] A. G. Warren, H. Brorson, L. J. Borud, S. A. Slavin. Lymphedema: A comprehensive review *Annals of Plastic Surgery* (2007) 59, 464-472.

[2] Vignes, S., Albuisson, J., Champion, L., Constans, J., Tauveron, V., Malloizel, J., Quéré, I., Simon, L., Arrault, M., Trévidic, P., Azria, P., Maruani, A. (2021). Primary lymphedema French National Diagnosis and Care Protocol (PNDS; Protocole National de Diagnostic et de Soins). *Orphanet Journal of Rare Diseases* (2021) , 16(1).

[3] Hayes, S. C., Janda, M., Ward, L. C., Reul-Hirche, H., Steele, M. L., Carter, J., Quinn, M., Cornish, B., Obermair, A. Lymphedema following gynecological cancer: Results from a prospective, longitudinal cohort study on prevalence, incidence and risk factors. *Gynecologic Oncology* (2017) 146(3), 623–629.

[4] Brix, B., Sery, O., Onorato, A., Ure, C., Roessler, A., Goswami, N. Biology of lymphedema. *In Biology* (2021) 10(4).

[5] Keast, D. H., Moffatt, C., Janmohammad, A. Lymphedema Impact and Prevalence International Study: The Canadian Data. *Lymphatic Research and Biology* (2019) 17(2).

[6] Rabe, E., Partsch, H., Hafner, J., Lattimer, C., Mosti, G., Neumann, M., Urbanek, T., Huebner, M., Gaillard, S., Carpentier, P. Indications for medical compression stockings in venous and lymphatic disorders: An evidence-based consensus statement. *Phlebology: The Journal of Venous Disease*, (2017) 33(3), 163–184.

[7] Ciudad, P., Sabbagh, M. D., Agko, M., Huang, T. C. T., Manrique, O. J., Román, C., Reynaga, C., Delgado, R., Maruccia, M., Chen, H.-C. Surgical Management of Lower Extremity Lymphedema: A Comprehensive Review. *Indian Journal of Plastic Surgery*, (2019) 52(1), 81–92.

[8] Sugisawa, R., Unno, N., Saito, T., Yamamoto, N., Inuzuka, K., Tanaka, H., Sano, M., Katahashi, K., Uranaka, H., Marumo, T., Konno, H. Effects of Compression Stockings on Elevation of Leg Lymph Pumping Pressure and Improvement of Quality of Life in Healthy Female Volunteers: A Randomized Controlled Trial. *Lymphatic Research and Biology* (2016) 14(2).

[9] Lim, C. S., Davies, A. H. Graduated compression stockings. CMAJ. *Canadian Medical Association Journal* (2014) 186(10)

[10] Rohan, P. Y., Badel, P., Lun, B., Rastel, D., Avril, S. Prediction of the Biomechanical Effects of Compression Therapy on Deep Veins Using Finite Element Modelling. *Annals of Biomedical Engineering* (2015) 43(2), 314–324.

[11] Avril, S., Badel, P., Dubuis, L., Rohan, P. Y., Debayle, J., Couzan, S., Pouget, J. F. Patient specific modeling of leg compression in the treatment of venous deficiency. Studies in Mechanobiology, *Tissue Engineering and Biomaterials* (2012) 9, 217–238.

[12] Rohan, C. P. Y., Badel, P., Lun, B., Rastel, D., Avril, S. Biomechanical response of varicose veins to elastic compression: A numerical study. *Journal of Biomechanics* (2013) 46(3), 599–603.

[13] Venkatesh, K. P., Raza, M. M., Kvedar, J. C. Health digital twins as tools for precision medicine: Considerations for computation, implementation, and regulation. *Digital Medicine* (2022) 5(1).

[14] Sun, T., He, X., Li, Z. Digital twin in healthcare: Recent updates and challenges. *Digital Health* (2023) 9:1-13.

[15] Johnson, P., Levine, S., Bonnard, C., Schuerer, K., Pécuchet, N., Gazères, N., D'Souza, K. Digital Twin for Healthcare and Lifesciences. *The Digital Twin* (2023) 1023–1044.

[16] Quarteroni, A., Manzoni, A., Negri, F. *Reduced basis methods for partial differential equations: An introduction*. (2015)

[17] Kast, M., Guo, M., Hesthaven, J. S. A non-intrusive multifidelity method for the reduced order modeling of nonlinear problems. *Computer Methods in Applied Mechanics and Engineering* (2020) 364, 112947.

[18] Chinesta, F., Cueto, E., Payan, Y., Ohayon, J. *Reduced Order Models for the Biomechanics of Living Organs* (2023).

[19] Lauzeral, N., Borzacchiello, D., Kugler, M., George, D., Rémond, Y., Hostettler, A., Chinesta, F. A model order reduction approach to create patient-specific mechanical models of human liver in computational medicine applications. *Computer Methods and Programs in Biomedicine* (2019) 170, 95–106.

[20] Demo, N., Tezzele, M., Rozza, G. A non-intrusive approach for the reconstruction of POD modal coefficients through active subspaces. *Comptes Rendus Mecanique* (2019) 347(11), 873–881.

[21] Salmoiraghi, F., Scardigli, A., Telib, H., Rozza, G. Free-form deformation, mesh morphing and reduced-order methods: enablers for efficient aerodynamic shape optimisation. *International Journal of Computational Fluid Dynamics* (2018) 32(4–5), 233–247.

[22] Mainini, L., Willcox, K. Surrogate modeling approach to support real-time structural assessment and decision making. *AIAA Journal* (2015) 53(6), 1612–1626.

[23] Avril, S. Hyperelasticity of Soft Tissues and Related Inverse Problems. *CISM International Centre for Mechanical Sciences* (2016) 573, 37–66.

[24] Dubuis, L., Avril, S., Debayle, J., Badel, P. Identification of the material parameters of soft tissues in the compressed leg. *Computer Methods in Biomechanics and Biomedical Engineering* (2012) 15(1), 3–11.

[25] Marinopoulos, T., Zani, L., Li, S., Silberschmidt, V. v. Modelling indentation of human lower-limb soft tissue: simulation parameters and their effects. *Continuum Mechanics and Thermodynamics* (2020) 35, 939-955.

[26] Verdugo, F., Badia, S. The software design of Gridap: a Finite Element package based on the Julia JIT compiler *Computer Physics Communications* (2022) 276, 108341.

[27] Liu, H., Ong, Y. S., Cai, J. A survey of adaptive sampling for global metamodeling in support of simulation-based complex engineering design. *In Structural and Multidisciplinary Optimization* (2018) 57(1), 393–416.

[28] Partsch, H., Winiger, J., Bertrand, L. Compression Stockings Reduce Occupational Leg Swelling. *Dermatologic Surgery* (2004) 30(5), 737-743.

[29] Nowicki, A., Dobruch-Sobczak, K. Introduction to ultrasound elastography. *J Ultrason.* (2006) 16(65), 113-124.